DEM Simulation of Shear Band Induced Foundation Rotation Due to the Reverse Fault - Shallow Foundation Interaction in Different Soil Densities

Author 1
- Saman Ghaderi, Ph.D. Student
- School of Civil Engineering, Iran University of Science and Technology, Tehran, Iran
- ORCID Number

Author 2
- Amir Mohammad Fahmi, M.Sc. Graduate
- School of Civil Engineering, Iran University of Science and Technology, Tehran, Iran
- ORCID Number

Author 3
- Alireza Saeedi Azizkandi*, Associate Professor
- School of Civil Engineering, Iran University of Science and Technology, Tehran, Iran
- ORCID Number

Corresponding Author: Alireza Saeedi Azizkandi, School of Civil Engineering, Iran University of Science and Technology, Tehran, Iran.

Tel: (+98) 2177240398

Email: asaeedia@iust.ac.ir

Abstract

During earthquakes, a pivotal process, known as 'fault rupture propagation' unfolds, involving the fracture of rock on the fault plane, advancing toward the ground surface. This phenomenon significantly affects nearby infrastructure upon contact with the ground. Shallow foundations, vital structures, that fall within their impact radius and their behavior while interacting with a fault should be studied. This study employs a 2D discrete element model, exploring reverse fault rupture-soil shallow foundation interaction in granular soils of varying densities. The research highlights the foundation's location as the most influential parameter affecting the characteristics of the formed shear band. Regardless of other factors, the shallow foundation consistently diverts fracture paths. As the footing's weight increases, this diversion intensifies. Regarding foundation rotation during faulting, increased weight and reduced distance from the fault's location generally mitigate rotation. Soil density's impact on rotation varies, causing a decrease in some cases and an increase in others. Also, by utilizing a proposed criterion, the safety of the foundation in interaction with reverse fault is evaluated and several tables have been made to predict the safety of the foundation under different conditions.

Keywords: Discrete Elements Modelling, Shallow Foundation Interaction, Reverse Fault, Shear Band

1. Introduction

Soil, with its inherent diversity and unpredictable characteristics, perpetually transforms due to the ever-changing environment. These variations, accrued over time, introduce a substantial degree of uncertainty into geotechnical considerations. One of the primary sources of this uncertainty stems from the formidable force of earthquakes, which give rise to two significant ground motion hazards. The first of these hazards is dynamic ground shaking, triggered by seismic waves traversing great distances. The second peril involves permanent ground deformation, induced by the fracturing of bedrock, commonly known as

earthquake surface fault rupture. This surface fault rupture represents a relatively quasi-static facet of fault displacement [1, 2]. It's important to note that not all seismic events result in surface fault ruptures[3]. However, when they do occur, they hold the potential to exert a profound influence on structures situated in proximity to the rupture path or even cause damage [4-13]. Post-earthquake observations have consistently shown that relatively massive or rigid structures with shallow foundations tend to exhibit robust performance under such conditions [8, 9]. It's worth noting that heavy foundations have been known to effectively alter the course of fault rupture [14-19].

The foundation of a structure assumes a pivotal role in determining its response to fault rupture. Structures constructed with rigid foundations demonstrate superior resilience compared to those relying on isolated foundations or piles [20-22]. Specifically, buildings characterized by stiff designs and supported by rigid box-type foundations exert substantial pressures at the ground surface, effectively coercing the fault rupture to deviate from its path and away from the foundation [8, 9]. Drawing from observations made in the aftermath of the Chi-Chi earthquake (1999), it became evident that heavy, well-reinforced concrete slab foundations wield a localized influence on the configuration of near-surface rupture's path [5, 15]. When a fault rupture fails to divert from the foundation, it can lead to foundation damage, marked by excessive rotation and the formation of voids beneath it [23, 24].

To explore the interaction between shallow foundations and faults, researchers conducted experimental model tests using a centrifuge. One of the initial studies aimed to assess how surface fault propagation behaves when a foundation is present on the ground surface in the context of both reverse and normal faults at a 60-degree angle. Parameters such as the weight, width, and position of the foundation concerning the fault's free field arrival conditions were examined in this study. The test results revealed a significant diversion of the fault's path due to the presence of the foundation, in comparison to scenarios without a foundation. It appears that a rigid and heavily loaded foundation should be positioned such that the fault intersects its center. The foundation's location relative to the fault proved to be one of the pivotal factors in foundation-fault interaction. A less loaded foundation, on the other hand, failed to divert the fault, failing the foundation [14].

Subsequent centrifuge tests were conducted to investigate the impact of the foundation's position on the interaction between reverse faulting and a surface foundation situated on sand. The findings demonstrated that the response of the foundation near the reverse fault is highly sensitive to its positioning in relation to the fault's emergence in a free field. Even when the fault's emergence is some distance away from the foundation, it can still lead to significant displacements of the foundation. The interaction between the foundation and the fault causes the fault's trajectory to diverge from what it would be in a free field. Three primary mechanisms of fault-foundation interaction come into play, depending on the foundation's position and the fault's displacement [14].

Within the realm of numerical modeling, numerous studies on the interaction between shallow foundations and faults have employed methods such as the Finite Element Method (FEM). The initial FEM study yielded results indicating that structures situated on continuous and sturdy mat or box-type foundations exhibit superior performance compared to those on isolated footings or piles. Buildings founded on continuous and rigid box-type foundations can even compel the outcropping rupture to change its course. Furthermore, an increase in the superstructure's dead load contributes to elevated stress levels beneath the foundation, subsequently enhancing the diversion of the dislocation [8, 9].

A subsequent study delved into the interaction between normal and reverse faulting when surface foundations are placed on homogeneous and undrained soil. This study identified three fundamental kinetic mechanisms used to predict fault deflection conditions caused by the presence of a foundation. Moreover, it derived a formula to assess the minimum load that a foundation must bear to alter the direction of a reverse or normal fault, independent of the fault type and its dip angle [25].

Yet another FEM study underscored the multitude of factors affecting foundation rotation in the context of surface faulting-foundation interaction. These factors include the relative position of the foundation to the fault path in free fields and the magnitude of the bearing pressure on the foundation [26].

As an alternative to the continuum approach, the Distinct Element Method (DEM) emerges as a notable technique, inherently equipped to capture phenomena associated with large strain localization. DEM is a numerical method designed to model the behavior of granular materials by representing them as discrete, interacting particles [27-29]. The Discrete Element Method (DEM) offers a robust approach for simulating shear band formation and strain localization. DEM models the material as an assembly of discrete particles

or blocks that interact through contact forces. This particle-based approach inherently captures the formation of shear bands and strain localization by allowing particles to interact and rearrange in response to applied loads. As the material deforms, the DEM can naturally represent the development of localized shear zones and the associated strain distribution.[2, 30] Researchers have harnessed the capabilities of DEM to simulate interactions between reverse and normal faults and surface foundations, as well as to scrutinize the influence of soil compaction on this interaction. The overarching conclusions drawn from these investigations concerning the impact of soil compaction and foundation load can be distilled as follows: as the load on the foundation increases, the degree of foundation rotation decreases while rupture deflection increases. Furthermore, an augmentation in soil compaction, within the specific foundation locations under scrutiny, leads to an increase in foundation rotation [31, 32].

In the current research, we focus on evaluating the safety of shallow foundations, specifically by examining foundation rotation and damage levels, under various conditions influenced by factors such as soil densities, foundation surcharge loads, fault dip angles, and the foundation's position relative to the fault path. While the effects of these factors on foundation safety have not been comprehensively and continuously investigated in previous studies, this paper aims to fill that gap. We employ the Distinct Element Method (DEM) to simulate conditions in sandy soil with two different relative densities. The study considers two distinct foundation surcharge loads, six different dip angles of the reverse fault, and examines the foundation's position at six different locations within the free field. Additionally, we provide comprehensive output data for different fault dislocation to soil height ratios (h/H), which can be utilized in engineering design. The primary goal is to investigate how these parameters affect the rupture path and foundation rotation, offering a deeper understanding of shallow foundation behavior in the presence of a reverse fault and ultimately assessing the safety of the foundation under these conditions.

2. Research Method

2.1. Steps to DEM Simulate a Soil-Shallow Foundation-Reverse Fault System

(1) Determination of Two-Dimensional (2D) Porosity

The utilization of two-dimensional (2D) plane strain modeling has become increasingly prevalent in geotechnical studies, primarily to streamline computational costs and reduce the time required for conducting tests. This approach is particularly valuable for modeling complex phenomena like the reverse fault phenomenon, as it offers valuable insights into key mechanisms and phenomena while minimizing computational overhead.

However, it's essential to recognize that when a 3D phenomenon is modeled in a 2D simulation, there are notable differences between the 2D area-based porosities and the 3D volume-based porosities (lab porosities) [33, 34]. While the porosities used in 3D DEM studies can be directly determined from laboratory porosities, those used in 2D DEM investigations require a different approach to be calculated based on laboratory porosities.

In the current study, to determine the 2D porosity, the procedure proposed by Wang et al. (2014) [34] was employed. This method involves a cyclic diagram procedure in which the 3D laboratory porosity of the soil is initially converted to 2D DEM porosity using a parabolic equation. Subsequently, a direct shear model is created, and the contact force distribution induced by the soil on the upper wall (F_{top}) of this model is measured. The F_{top} criterion should ideally fall between 0 and 1% of the specimen weight ($G_{specimen}$). The behavior of the top wall is influenced by F_{top}, where it moves upwards if F_{top} exceeds 1% of the sample weight and downwards if F_{top} is equal to 0.

Through this procedure, the 2D porosities of Firoozkoh sand No. 161 (with e_{max} = 0.943 and e_{min} = 0.603) [35, 36] are calculated. These 2D porosities were found to be 0.184 for loose sand (with a relative density of 60%) and 0.157 for dense sand (with a relative density of 95%). The calculation of these porosities involved an iterative procedure employing trial and error to achieve the desired porosity and realistic contact force distribution.

(2) Geometry of the Model and Construction of Porous Sample

Figure.1 provides an illustration of the Soil-Shallow Foundation-Reverse Fault System's geometry. The testing box encompasses a uniform soil layer with dimensions of width B and height H. A fault rupture with a dipping angle β extends to the bottom of the sand layer at point O. The testing box's boundaries are defined by five rigid wall elements, as depicted in Figure.1. These boundaries include the footing walls (walls 1 and 3), which are fixed in the x and y directions, and the boundary walls of the hanging wall, which are movable in both directions.

To generate soil particles within the testing box, a random number function is utilized to create the required number of particles with random coordinates inside the box. The quantity and diameters of these particles are determined based on the Particle Size Distribution (PSD) curve of the chosen assembly. The diameters are scaled up to be five and eight times larger than the experimental curve of the Firoozkuh sand no. 161 [35, 36] as shown in Figure.2. This up-scaling is a common technique in DEM studies to reduce computation time by reducing the number of particles and contacts [30-32, 37]. Another approach to reduce computation time is to fill the center of the box with a PSD curve five times larger than the experimental curve (finer particles) because most of the study and induced tension occurs in the middle of the testing box. The sides of the box are filled with a PSD curve eight times larger than the experimental curve. This approach aligns with the work of Garcia and Bray [31, 32, 38].

To create the soil specimen, a sand layer is deposited within the fault box using the sedimentation approach. In this method, sand particles settle under gravity's influence until they reach a stable equilibrium condition and achieve the desired porosity, mirroring natural sedimentation processes [39]. The gravitational acceleration is set to an appropriate value, such as 50g, for simulating a 1/50th-scale geotechnical centrifuge model test, where g represents the standard gravitational acceleration of 9.81 m/s². A quasi-static simulation is performed by incrementally applying gravitational acceleration to the particles in 106 steps.

A crucial step in this compaction process is assigning the initial contact model to the particles. Initially, the linear contact model is used to represent inter-particle interactions. This model depicts an infinitesimal interface that allows relative rotation (there is no resistance) and leads to faster compaction and reduced computation time. The micro material parameters for the compaction stage are calibrated and provided in Table.1, with details of the calibration and verification discussed in the subsequent section.

(3) Modifying the Particle Contact Model

Following the compaction process, once the specimen has reached a stable equilibrium condition and the desired porosity, it becomes essential to adjust the inter-particle contact model to accurately depict the macro behavior of Firoozkoh sand No. 161. The commonly employed contact model for granular soils is the rolling resistance linear model, which incorporates a rolling resistance mechanism into the linear contact model. This model effectively compensates for the assumption of particle circularity and appropriately represents the rough and uneven surfaces of sand particles to a considerable extent [40, 41]. The calibrated micro parameters for this modified contact model are presented in Table.1. As mentioned earlier, the details of the calibration and verification processes employed to determine these parameters will be discussed in the subsequent section.

(4) Creating the Shallow Foundation

To simulate these shallow foundations, four rows of particles are generated in an organized arrangement, and the inter-particle contact model between these particles is implemented using the linear parallel bond contact model. These particles are assembled in a rectangular shape, and the contact model is applied to them to represent the behavior of the foundation. The micro parameters employed for simulating these shallow foundations are summarized in Table.2. The foundation pressure is also simulated by considering the weight of the foundation. Through a trial-and-error process, the stiffness of the foundation particles was set to four times greater than that of the soil, with tensile strength and cohesion values 4,000 and 400,000 times greater, respectively. This process was crucial to ensure that the foundation's particles exhibit no relative displacement during faulting, confirming that the foundation behaves as a rigid body throughout the simulations.

(5) Faulting Process

To simulate reverse faulting, the boundaries of the hanging wall are displaced incrementally in parallel with the fault plane (β). Since fault rupture propagation is essentially a quasi-static phenomenon [1], the required vertical displacement (h) is applied in a series of sequential steps at a controlled speed of approximately 0.01 m/s (equivalent to 10-7 meters per computational step). This ensures that the specimen remains in quasi-static conditions throughout the simulation. In order to monitor and control the quasi-static response of the specimen, the Ratio Average (R_{ave}) is measured during the simulation. In all simulations, R_{ave} should remain below 0.01, indicating quasi-static fault rupture [42]. The faulting process continues until the desired displacement of the fault is achieved which for this study is vertical bedrock displacement (h) relative to soil height (H) of h/H = 20%. During the faulting process, the rotation of the foundation is also recorded, providing valuable data for the analysis.

2.2. Verification and Calibration of Micro Parameters of Inter-Particle Contact Model

The PFC2D software program developed by Itasca Consulting Group in 2018 was employed for modeling the complex soil-shallow foundation-reverse fault system. Rigorous verification and calibration of the PFC2D the micro parameters of the rolling resistance linear contact model, the inter-particle model, were conducted through two experimental investigations.

The first experiment involved a centrifuge model simulating reverse faulting with a dip angle (β) of 75° on loose Firoozkoh sand No. 161, as detailed by [36]. The centrifuge model, scaled at 1/50th, featured dimensions of B = 0.63 m and H = 0.24 m, incorporating 79569 particles. Figure.3(b) visually depicts the fault rupture in the Discrete Element Method (DEM) model, showcasing particles with a rotation exceeding 0.5 radians post-faulting, illustrating the propagation of the shear band of the fault in the soil. The simulated fault rupture closely aligns with the experimental observations, with both exhibiting convex fault ruptures when viewed from the hanging wall. The vertical displacements of the ground surface at the prototype scale, compared between the experiment and DEM prediction in Figure.3(c), reveal a highly satisfactory agreement.

The second experiment, conducted by [24], focused on a model with a dip angle (β) of 60° and a shallow foundation on loose sand, mirroring the properties of the previous test. The foundation pressure in this scenario was q = 81 KPa. Figure.4(a) and (b) presents a comparison of fault ruptures between the centrifuge experiment and the DEM study, demonstrating the accurate simulation of general centrifuge model behavior. The foundation rotation during faulting is explored in Figure.4(c), revealing a highly satisfactory correlation between experimental results and DEM predictions, particularly in illustrating the consistent increase in foundation rotation with fault displacements.

As mentioned before to maintain a quasi-static condition throughout the simulations, the fault movement was deliberately applied at a slow pace, limiting the maximum fault velocity to approximately 0.01 m/s. Monitoring the ratio average (R_{ave}) during faulting, as depicted in Figure.5(a) and Figure.5(b), consistently indicated that R_{ave} remained below 0.01 throughout the faulting process, affirming the appropriateness of the simulation speed for maintaining quasi-static conditions.

The micro parameters of the contact models listed in Table.1 were carefully selected based on the insights gained from these simulations. The objective was to accurately replicate the macro behavior of Firoozkoh sand No. 161, ensuring a close alignment between the simulated and observed behaviors at the macro level.

2.3. Testing Program

A comprehensive series of 144 tests were systematically conducted to investigate the repercussions of a reverse fault on a shallow foundation. This meticulous examination took into consideration various critical factors, as outlined below:

- **Soil Density**

The study utilized Firoozkoh sand No. 161, with a deliberate exploration of two distinct density conditions:

Loose sand (denoted by L) with a Relative Density (DR) of 60%.
Dense sand (denoted by D) with a Relative Density (DR) of 95%.

● **Fault Dip Angles**

To scrutinize the impact of fault dip angles, six different angles were incorporated into the study:
β=15°, 30°, 45°, 60°, 75°, and 90°.

● **Foundation Weight**

Two types of foundations were employed to assess the effect of foundation weight:
Light foundation (denoted by L) with a foundation pressure (q) of 81 kPa.
Heavy foundation (denoted by H) with a foundation pressure (q) of 162 kPa.

● **Position of the Foundation**

The s/b parameter was introduced to investigate the influence of the foundation's position relative to the fault. Here, the s parameter represents the distance between the free field fault rupture and the left corner of the foundation, while the b parameter corresponds to the width of the foundation. Six distinct positions were considered:
s/b = -0.25, 0.00, 0.25, 0.50, 0.75, and 1.00.

The analyses are subsequently denoted as R (dip) (soil density) (foundation weight) (s/b), where R stands for Reverse fault. For example, R15LL(-0.25) refers to a reverse fault with a dip angle of 15°, in loose sand with a light foundation, and a s/b location of -0.25. This systematic nomenclature provides a clear and concise reference to the specific conditions under investigation in each test.

3. Results and Discussion

3.1. Shear Band Formation

Figures.6-11 vividly illustrate particles with a rotation exceeding 0.5 radians for various fault dip angles, soil types, foundation types, and locations. Notably, the width of the shear band is observed to be wider in loose sands across these figures.

In models with a lower dip angle of 45°, a distinctive back-thrust shear band manifests, propagating through the moving block (hanging wall). This shear band exhibits convexity when viewed from the footing wall. The width of this shear band widens in loose sands, especially with a decrease in the s/b value (when the foundation is closer to the fault) and when the foundation is heavier. In the faults with the dip angle of 45°, the back-thrust shear band is also formed in R45LH(0.25), R45DH(-0.25), R45DH(0.00), and R45DH(0.25) which shows the formation's dependency to the soil density, foundation weight, and the s/b value.

Across all figures, it becomes evident that shallow foundations in the models deflect the path of rupture, and with an increase in foundation weight, this deflection intensifies. The deviation tends to occur primarily towards the two corners of the shallow foundation.

In the fault with a dip angle of 15° (Figure.6) in loose soil and with a light foundation in the s/b ratios of -0.25, 0.00, 0.25, and 0.50, a unique scenario unfolds where the propagated shear band toward the fixed block divides into two paths (in the s ratio s/b = 0.50, the division is not complete). A part of the shear band deviates towards the right corner of the shallow foundation so that when is seen from the side of the moving block, it is convex; But the second part of the shear band spreads to the bottom of the left corner of the shallow foundation with downward concavity, and then it turns into two branches, one of which spreads to the left corner of the footing and the other to the fixed block. The bifurcation is more pronounced in heavy foundation models and less dispersed in dense soil. This splitting phenomenon is exclusive to specific s/b ratios, emphasizing the intricate interplay between foundation characteristics and soil conditions. Splitting of the shear band in loose soil with heavy foundation occurs only in s/b ratios of -0.25, 0.00, and 0.25 (although in the s/b = 0.25 ratio, the formation of the second rupture towards the left corner of the foundation is not complete).

For the fault with a 30° angle (Figure.7), similar to the 15° models, in the loose soil with a light foundation the separation and bifurcation of the shear band occur in select s/b ratios of -0.25, 0.00, and

0.25, and In models with loose soil and heavy foundation it occurs in s/b ratios of -0.25 and 0.00 (although the formation of ruptures towards the left corner of the foundation is not complete in the ratio s/b = 0.00). In the models with dense soil and light footing, separation and splitting of the footing shear band occurs at an s/b ratio of -0.25 and 0.00, and also in models with dense soil and heavy footing, this happens only at the ratio of s/b = -0.25.

At a fault angle of 45° (Figure.8), separation and bifurcation are observed in R45LL(-0.25), R45LL(0.00), R45LH(-0.25), R45LH(0.00), R45DL(-0.25), R45DL(0.00), R45DH(-0.25), and R45DH(0.00) models, with the shear band deviating towards both the right and left corners of the foundation. The formation of concave and convex ruptures, particularly in heavy foundation models, underscores the complex behavior influenced by fault angles and foundation characteristics.

In the fault with a 60° angle (Figure.9), the shear band splits into two parts in R60LL(-0.25), R60LL(0.00), R60LL(0.25), R60LH(-0.25), R60LH(0.00), R60LH(0.25), R60DL(-0.25), R60DL(0.00), R60DL(0.25), R60DH(-0.25), R60DH(0.00) models, showing concave deviation towards the right corner and bifurcation towards the left corner. Heavy foundations further accentuate these features.

At a 75° fault angle (Figure.10), separation, and bifurcation occur in select s/b ratios of -0.25, 0.00, and 0.25 in both loose and dense soil with light and heavy foundations, resembling the patterns observed at a 60° angle. However, an intriguing rupture forms from the left corner towards the moving block in models with s/b = -0.25 which intercepts with the right corner shear band formation.

For a fault angle of 90° (Figure.11), separation and splitting of the shear band are evident in specific s/b ratios of -0.25, 0.00, and -0.25 in loose and dense soil, with ruptures towards both the left and right corners of the foundation. Complex patterns emerge, showcasing the intricate interplay between fault angles, soil characteristics, and foundation attributes.

3.2. Parameter Influencing the Rotation of the Foundation

3.2.1. The Weight of the Foundation and the Soil Density

In Figures S.1-6, a consistent trend is observed across all graphs, whether in loose or dense soil, as the shallow foundation's weight increases, the foundation rotation decreases. This pattern is evident in all fault angles except for 90 degrees, where, in the case of s/b = 1.00, the rotation of the heavy foundation surpasses that of the light foundation. This divergence is likely attributed to the greater tendency of particles to escape from the corners of the heavier foundation compared to the lighter one.

The influence of soil compaction varies across models. In the fault with a 15-degree angle (Figure S.1) and a light foundation, foundation rotation in different s/b ratios remains nearly the same in both loose and dense soils, with minimal changes. However, in models with a heavy foundation in the ratio s/b values of -0.25 and 0.50 foundation rotation in dense soil is less than in loose soil, and in the s/b ratio of 0.00 and 0.25, up to about 16% of the strain, the rotation in dense soil is less than loose soil and after that rotation in Dense soil becomes greater than loose soil; However, in the s/b ratio of 0.75 and 1.00, up to about 16% strain in dense soil is more than in loose soil, and then as the faulting continues, it becomes less than loose soil.

At a fault angle of 30 degrees (Figure S.2), foundation rotation in dense soil, except for s/b = -0.25, is consistently less than in loose soil. This holds true for models with both light and heavy foundations, except for the s/b = -0.25 scenario where rotations are almost identical in both soil types with the light foundation.

For a fault angle of 45 degrees (Figure S.3), in all s/b ratios except s/b=1.00, the rotation of the shallow foundation in dense soil is less than in loose soil. Only in models with s/b=1.00 is the rotation in dense soil slightly more than in loose soil at the beginning of the fault.

In the fault with a 60-degree angle (Figure S.4), foundation rotation in dense soil is less than in loose soil for models with a light foundation and s/b = -0.25. However, for models with a heavy foundation, rotation in dense soil is more than in loose soil. In ratio s/b = 0.00, the rotation of the shallow foundation in both types of models with light and heavy foundations in dense soil is more than in loose soil, and only in the model with heavy foundation, around 16% strain, the rotation in dense soil is less than that in loose soil. In the models with s/b = 0.25 ratio, in the models with light foundation, the rotation in dense soil is more than in loose soil, while in the models with heavy foundation, up to 16% strain, the rotation in dense

soil is more than in loose soil, and then the trend gets reversed. But in the s/b ratios of 0.50, 0.75, and 1.00, the rotation with both types of light and heavy foundations is lesser in the dense soil.

For a fault angle of 75 degrees (Figure S.5), in s/b ratios of -0.25 and 0.00, foundation rotation in dense soil is less than in loose soil. However, in s/b ratios of 0.25, 0.50, and 0.75, rotation in dense soil surpasses that in loose soil. Notably, in the s/b=0.75 scenario with a light foundation, rotations in both loose and dense soils are almost identical.

In the fault with a 90-degree angle (Figure S.6), only in the s/b = -0.25 scenario is the rotation of the foundation in dense soil less than in loose soil. In other s/b ratios, foundation rotation in dense soil exceeds that in loose soil.

It is noteworthy that in models with insignificant foundation rotation (s/b = 1.00), the fluctuating nature of the rotation diagrams is attributed to the escape of coarse particles from under the foundation corners, causing clockwise and counterclockwise rotations of the foundation.

3.2.2. The Location of the Foundation

In Figures S.7-12, a consistent trend is observed across most models in which an increase in the s/b ratio correlates with a decrease in shallow foundation rotations. However, certain exceptions are noted, particularly in models with fault angles of 60, 75, and 90 degrees, where models with an s/b = -0.25 ratio exhibit less rotation than those with greater s/b ratios.

In loose soil with a light foundation and fault angles of 60 degrees, models with an s/b = -0.25 ratio, after about half the applied strain, demonstrate less foundation rotation than models with s/b = 0.00. Additionally, these models exhibit lower foundation rotation at the end of the applied strain compared to those with an s/b = 0.25 ratio. For loose soil with a heavy foundation, the model with an s/b = -0.25 ratio has less foundation rotation than the model with s/b = 0.00 from about 8% strain onwards. In dense soil with a light foundation, the model with an s/b = -0.25 ratio, from about 4% strain, demonstrates less foundation rotation than models with s/b = 0.00 and 0.25. Additionally, at the 8% strain range, the model with an s/b = 0.25 ratio has slightly more rotation than the model with s/b = 0.00. In dense soil with a heavy foundation, the model with an s/b = -0.25 ratio has less foundation rotation than the model with s/b = 0.00 (Figure S.10).

In a fault angle of 75 degrees with loose soil with a light foundation, the model with an s/b = -0.25 ratio, has less foundation rotation than models with s/b = 0.00 and 0.25. For models with dense soil and light foundation the model with an s/b = -0.25 ratio, from 4% strain onwards, displays less foundation rotation than models with s/b = 0.00 and 0.25 ratios. Moreover, from 12% strain onwards, this model exhibits less foundation rotation than the model with s/b = 0.50. Also, in the model with dense soil and heavy foundation, an s/b = 0.25 ratio has more rotation than the model with an s/b = 0 from the beginning of the strain application. Additionally, from 12% strain onwards, this model has more rotation than the model with an s/b = -0.25 ratio (Figure S.11).

In models with a fault angle of 90 degrees in dense soil with both foundations, the model with an s/b = -0.25 ratio has less foundation rotation than models with an s/b = 0.00 and 0.25 (Figure S.12).

3.3. Shallow Foundation Safety Evaluation

In order to assess the structural integrity of foundations when subjected to the influence of a reverse fault, Baziar et al. (2019) [43] have proposed a comprehensive criterion, as detailed in Table.3. This criterion reveals that if the foundation undergoes a rotation exceeding 2 degrees during the faulting process, the resultant damage escalates to a severe level. Furthermore, when the rotation surpasses 5 degrees, the stability of the foundation is jeopardized.

Applying this criterion, an in-depth analysis of the rotation graphs for various foundation types, locations, and soil types is conducted during reverse faults with a displacement ratio of h/H = 20% (where H represents the height of the testing box). The values of h/H (%) corresponding to the critical 2° rotations of the foundation are meticulously documented in Tables.4-9 for each fault dip angle considered in this study.

These tables serve as invaluable tools for predictive assessment, enabling stakeholders to determine the safety of a foundation based on factors such as fault dip angle, fault displacement, soil type, foundation type, and the foundation's proximity to the fault. In instances where a foundation is deemed unsafe, these

findings prompt careful consideration of appropriate enhancements to ensure the robustness and stability of both the foundation and its supporting superstructure.

4. Conclusion

The study on the interaction of reverse faults in granular soil with shallow foundations using the DEM algorithm reveals several key findings:

1. **Shear Band Characteristics and Soil Density**: An increase in soil density and foundation weight leads to a reduction in shear band width and dispersion. This emphasizes the significant impact of these parameters on localized failure mechanisms.
2. **Rupture Mechanisms and s/b Ratio**: The primary rupture mechanism is strongly influenced by the s/b ratio, especially at lower ratios where the failure mechanism tends toward bifurcation, highlighting the critical role of the s/b ratio in shaping the rupture path.
3. **Back-Thrust Shear Band Formation**: For faults with dip angles below 45 degrees, a back-thrust shear band develops towards the moving block. Its width increases with decreasing soil density and s/b value, and its formation is notably influenced by the s/b ratio, particularly at a fault angle of 45 degrees.
4. **Foundation Weight and Rupture Deviation**: Heavier foundations exhibit greater rupture deviation, with the shear band deviating to the left corner of the foundation and forming two branches at larger distances. This highlights the impact of foundation weight on rupture behavior.
5. **Concavity of Shear Bands**: The back-thrust shear band consistently shows concavity towards the moving block. The segment deviating to the right corner displays concavity towards the moving block, while the part deviating towards the left corner shows downward concavity until bifurcation.
6. **Foundation Safety and s/b Ratio**: A comprehensive assessment of foundation safety under various conditions, using the criterion proposed by Baziar et al. (2019)[43], reveals crucial insights. The study provides tables with strain values corresponding to critical safety criteria, offering valuable information for designers and engineers to ensure foundation stability and security during interactions with reverse faults. This emphasizes the importance of considering fault dynamics, foundation characteristics, and soil conditions for effective foundation design.

These findings offer significant insights into shallow foundation behavior interacting with reverse faults, focusing on shear band formation, foundation rotation, and critical safety considerations.

The supplementary data is available at:

file:///C:/Users/pc/Downloads/Supplementary%20Data-9011.pdf

References

1. Loukidis, D., G.D. Bouckovalas, and A.G. Papadimitriou, "Analysis of fault rupture propagation through uniform soil cover". *Soil Dynamics and Earthquake Engineering*, 2009. **29**(11-12): p. 1389-1404. DOI: https://doi.org/10.1016/j.soildyn.2009.04.003.
2. Ghaderi, S. and A. Saeedi Azizkandi, "Micro–macro analysis of shear band formation in various normalised reverse fault throws". *Proceedings of the Institution of Civil Engineers-Geotechnical Engineering*, 2023: p. 1-18. DOI: https://doi.org/10.1680/jgeen.22.00095.
3. Garcia, F.E. and J.D. Bray, "Discrete element analysis of earthquake surface fault rupture through layered media". *Soil Dynamics and Earthquake Engineering*, 2022. **152**: p. 107021. DOI: https://doi.org/10.1016/j.soildyn.2021.107021.
4. Bray, J.D., R.B. Seed, L.S. Cluff, et al., "Earthquake fault rupture propagation through soil". *Journal of Geotechnical Engineering*, 1994. **120**(3): p. 543-561. DOI: https://doi.org/10.1061/(ASCE)0733-9410(1994)120:3(543).
5. Chen, C.-C., C.-T. Huang, R.-H. Cherng, et al., "Preliminary investigation of damage to near fault buildings of the 1999 Chi-Chi earthquake". Earthquake Engineering and Engineering Seismology. Vol. 2. 2000. 79-92. Link: https://www.ctsee.org.tw/pdf/ee0201/es0201-5.pdf.
6. ULUSAY, R., Ö. AYDAN, and M. HAMADA, "The behaviour of structures built on active fault zones: examples from the recent earthquakes of Turkey". *Structural Engineering/Earthquake Engineering*, 2002. **19**(2): p. 149s-167s. DOI: https://doi.org/10.2208/jsceseee.19.149s.

7. Dong, J., C. Wang, C. Lee, et al., "The influence of surface ruptures on building damage in the 1999 Chi-Chi earthquake: a case study in Fengyuan City". *Engineering Geology*, 2004. **71**(1-2): p. 157-179. DOI: https://doi.org/10.1016/S0013-7952(03)00131-5.
8. Anastasopoulos, I. and G. Gazetas, "Foundation–structure systems over a rupturing normal fault: Part I. Observations after the Kocaeli 1999 earthquake". *Bulletin of Earthquake Engineering*, 2007. **5**(3): p. 253-275. DOI: https://doi.org/10.1007/s10518-007-9029-2.
9. Anastasopoulos, I. and G. Gazetas, "Foundation–structure systems over a rupturing normal fault: Part II. Analysis of the Kocaeli case histories". *Bulletin of Earthquake Engineering*, 2007. **5**(3): p. 277-301. DOI: https://doi.org/10.1007/s10518-007-9030-9.
10. Zhang, Z., Y. Zhang, R. Wei, et al., "The damage mode and forced response characteristics of articulated lining structure: A case study of metro tunnel under a reverse fault action". *Tunnelling and Underground Space Technology*, 2023. **140**: p. 105246. DOI: https://doi.org/10.1016/j.tust.2023.105246.
11. Zhao, Y., G. Jiang, X. Lei, et al., "The 2021 Ms 6.0 Luxian (China) earthquake: Blind reverse-fault rupture in deep sedimentary formations likely induced by pressure perturbation from hydraulic fracturing". *Geophysical Research Letters*, 2023. **50**(7): p. e2023GL103209. DOI: https://doi.org/10.1029/2023GL103209.
12. Shidloon, A., M. Ashtiani, and A. Ghalandarzadeh, "Numerical modeling of trench adjacent to a shallow foundation for mitigating reverse fault rupture effects". *European Journal of Environmental and Civil Engineering*, 2024. **28**(8): p. 1850-1874. DOI: https://doi.org/10.1080/19648189.2023.2282556.
13. Zhang, X., L. Yu, M. Wang, et al., "Mechanical response and failure characteristics of tunnels subjected to reverse faulting with nonuniform displacement: Theoretical and numerical investigation". *Engineering Failure Analysis*, 2024. **156**: p. 107809. DOI: https://doi.org/10.1016/j.engfailanal.2023.107809.
14. Bransby, M., M. Davies, A. El Nahas, et al., "Centrifuge modelling of reverse fault–foundation interaction". *Bulletin of Earthquake Engineering*, 2008. **6**(4): p. 607-628. DOI: https://doi.org/10.1007/s10518-008-9080-7.
15. Faccioli, E., I. Anastasopoulos, G. Gazetas, et al., "Fault rupture–foundation interaction: selected case histories". *Bulletin of Earthquake Engineering*, 2008. **6**(4): p. 557-583. DOI: https://doi.org/10.1007/s10518-008-9089-y.
16. Ma, C., X. Cheng, T. Xu, et al., "Research on local buckling failure range of X80 buried steel pipeline under oblique-reverse fault". *Soil Dynamics and Earthquake Engineering*, 2023. **164**: p. 107592. DOI: https://doi.org/10.1016/j.soildyn.2022.107592.
17. Tao, L., Z. Wang, C. Shi, et al., "Investigation of the longitudinal mechanical response of pipeline or tunnel under reverse fault dislocation". *Rock Mechanics and Rock Engineering*, 2023. **56**(9): p. 6237-6259. DOI: https://doi.org/10.1007/s00603-023-03371-7.
18. Wang, Z., L. Tao, C. Shi, et al., "Response and failure mechanism of utility tunnel with flexible joints under reverse fault: An experimental, numerical, and analytical investigation". *Earthquake Spectra*, 2023. **39**(1): p. 335-361. DOI: https://doi.org/10.1177/87552930221143144.
19. Wang, Z., M. Zhao, J. Huang, et al., "Numerical modeling of reverse fault rupture and its impact on mountain tunnels". *Journal of Earthquake Engineering*, 2023. **27**(9): p. 2481-2505. DOI: https://doi.org/10.1080/13632469.2022.2121332.
20. Oettle, N.K. and J.D. Bray, "Geotechnical mitigation strategies for earthquake surface fault rupture". *Journal of Geotechnical and Geoenvironmental Engineering*, 2013. **139**(11): p. 1864-1874. DOI: https://doi.org/10.1061/(ASCE)GT.1943-5606.0000933.
21. Chiama, K., B. Chauvin, A. Plesch, et al., "Geomechanical Modeling of Ground Surface Deformation Associated with Thrust and Reverse-Fault Earthquakes: A Distinct Element Approach". *Bulletin of the Seismological Society of America*, 2023. **113**(4): p. 1702-1723. DOI: https://doi.org/10.1785/0120220264.
22. Chiang, J., E.E. Michel, K.-H. Yang, et al., "Mitigation of reverse faulting in foundation soils using geosynthetic-encased granular columns". *Transportation Geotechnics*, 2023. **42**: p. 101067. DOI: https://doi.org/10.1016/j.trgeo.2023.101067.
23. Ahmed, W. and M.F. Bransby, "Interaction of shallow foundations with reverse faults". *Journal of geotechnical and geoenvironmental engineering*, 2009. **135**(7): p. 914-924. DOI: https://doi.org/10.1061/(ASCE)GT.1943-5606.0000072.
24. Ashtiani, M., A. Ghalandarzadeh, and I. Towhata, "Centrifuge modeling of shallow embedded foundations subjected to reverse fault rupture". *Canadian Geotechnical Journal*, 2015. **53**(3): p. 505-519. DOI: https://doi.org/10.1139/cgj-2014-0444.
25. Tolga Yilmaz, M., R.J.E.e. Paolucci, and s. dynamics, "Earthquake fault rupture—shallow foundation interaction in undrained soils: a simplified analytical approach". *Earthquake engineering and structural dynamics*, 2007. **36**(1): p. 101-118. DOI: https://doi.org/10.1002/eqe.625.
26. Baziar, M.H., A. Nabizadeh, and M. Jabbary, "Numerical modeling of interaction between dip-slip fault and shallow foundation". *Bulletin of Earthquake Engineering*, 2015. **13**(6): p. 1613-1632. DOI: https://doi.org/10.1007/s10518-014-9690-1.
27. Cundall, P.A. and O.D. Strack, "A discrete numerical model for granular assemblies". *Geotechnique*, 1979. **29**(1): p. 47-65. DOI: https://doi.org/10.1680/geot.1979.29.1.47.
28. Garcia, F.E., E. Andò, G. Viggiani, et al., "Influence of depositional fabric on mechanical properties of naturally deposited sands". *Géotechnique*, 2022: p. 1-15. DOI: https://doi.org/10.1680/jgeot.21.00230.
29. Hazeghian, M. and A. Soroush, "DEM-aided study of Coulomb and Roscoe theories for shear band inclination". *Acta Geotechnica*, 2022. **17**(8): p. 3357-3375. DOI: https://doi.org/10.1007/s11440-022-01475-y.
30. Hazeghian, M. and A. Soroush, "Numerical modeling of dip-slip faulting through granular soils using DEM". *Soil Dynamics and Earthquake Engineering*, 2017. **97**: p. 155-171. DOI: https://doi.org/10.1016/j.soildyn.2017.03.021.
31. Garcia, F.E. and J.D. Bray, "Distinct element simulations of earthquake fault rupture through materials of varying density". *Soils and foundations*, 2018. **58**(4): p. 986-1000. DOI: https://doi.org/10.1016/j.sandf.2018.05.009.
32. Garcia, F.E. and J.D. Bray, "Distinct element simulations of shear rupture in dilatant granular media". *International Journal of Geomechanics*, 2018. **18**(9): p. 04018111. DOI: https://doi.org/10.1061/(ASCE)GM.1943-5622.0001238.

33. O'Sullivan, C., "Particulate discrete element modelling: a geomechanics perspective". 2011: CRC Press Taylor & Francis group. DOI: https://doi.org/10.1201/9781482266498.
34. Wang, Z., A. Ruiken, F. Jacobs, et al., "A new suggestion for determining 2D porosities in DEM studies". *Geomechanics and Engineering*, 2014. **7**(6): p. 665-678. DOI: https://doi.org/10.12989/gae.2014.7.6.665.
35. Ashtiani, M., A. Ghalandarzadeh, M. Mahdavi, et al., "Centrifuge modeling of geotechnical mitigation measures for shallow foundations subjected to reverse faulting". *Canadian Geotechnical Journal*, 2018. **55**(8): p. 1130-1143. DOI: https://doi.org/10.1139/cgj-2017-0093.
36. Saeedi Azizkandi, A., M.H. Baziar, S. Ghavami, et al., "Use of Vertical and Inclined Walls to Mitigate the Interaction of Reverse Faulting and Shallow Foundations: Centrifuge Tests and Numerical Simulation". *Journal of Geotechnical Geoenvironmental Engineering*
2020. **147**(2): p. 04020155. DOI: https://doi.org/10.1061/(ASCE)GT.1943-5606.0002433.
37. Hazeghian, M. and A. Soroush, "DEM-aided study of shear band formation in dip-slip faulting through granular soils". *Computers and Geotechnics*, 2016. **71**: p. 221-236. DOI: https://doi.org/10.1016/j.soildyn.2017.03.021.
38. Garcia, F.E. and J.D. Bray, "Discrete-element analysis of influence of granular soil density on earthquake surface fault rupture interaction with rigid foundations". *Journal of Geotechnical and Geoenvironmental Engineering*, 2019. **145**(11): p. 04019093. DOI: https://doi.org/10.1061/(ASCE)GT.1943-5606.0002163.
39. O'Sullivan, C. "Advancing geomechanics using DEM". in *The International Symposium on Geomechanics from Micro to Macro (IS-Cambridge 2014)*. 2014. Link: https://is-cambridge.eng.cam.ac.uk/system/files/documents/Catherine_OSullivan.pdf.
40. Iwashita, K. and M. Oda, "Rolling resistance at contacts in simulation of shear band development by DEM". *Journal of engineering mechanics*, 1998. **124**(3): p. 285-292. DOI: https://doi.org/10.1061/(ASCE)0733-9399(1998)124:3(285).
41. Wensrich, C. and A. Katterfeld, "Rolling friction as a technique for modelling particle shape in DEM". *Powder Technology*, 2012. **217**: p. 409-417. DOI: https://doi.org/10.1016/j.powtec.2011.10.057.
42. Itasca Consulting Group, I., *PFC — Particle Flow Code, Ver. 6.0*. 2018, Minneapolis: Itasca.
43. Baziar, M.H., S.H. Hasanaklou, and A.S. Azizkandi, "Evaluation of EPS wall effectiveness to mitigate shallow foundation deformation induced by reverse faulting". *Bulletin of Earthquake Engineering*, 2019. **17**(6): p. 3095-3117. DOI: https://doi.org/10.1007/s10518-019-00581-9.

Table Caption List

Table.1. Calibrated micro parameters of the soil particles contact models
Table.2. Micro parameters of the shallow foundation particles contact models
Table.3. Rotation limits and corresponding damage levels [43]
Table.4. Values of h/H (%) corresponding to the critical 2° foundation rotations for the reverse fault with $\beta = 15°$
Table.5. Values of h/H (%) corresponding to the critical 2° foundation rotations for the reverse fault with $\beta = 30°$
Table.6. Values of h/H (%) corresponding to the critical 2° foundation rotations for the reverse fault with $\beta = 45°$
Table.7. Values of h/H (%) corresponding to the critical 2° foundation rotations for the reverse fault with $\beta = 60°$
Table.8. Values of h/H (%) corresponding to the critical 2° foundation rotations for the reverse fault with $\beta = 75°$
Table.9. Values of h/H (%) corresponding to the critical 2° foundation rotations for the reverse fault with $\beta = 90°$

Tables

Table.1

Parameters	Compaction stage (Linear Model)	Faulting stage (Rolling Resistance Linear Model)
Inter-particle elasticity modulus, E^*: MPa	100	100
Normal-to-shear stiffness ratio, κ^*	0.2	0.2
Inter-particle friction, μ	0.3 (Loose Sand)	0.3
	0.05 (Dense Sand)	0.3
Wall-particle friction, μ_{wall}	0	0.3
Inter-particle rolling friction coefficient, μ_r	-	0.2
Non-local damping coefficient, α_d	0.7	0.1
Normal critical damping ratio, β_n	0.2	Not considered

Shear critical damping ratio, β_s	0.2	Not considered
Particle density, M: kg/m^3	2670	2670

٥٥٤
٥٥٥
٥٥٦
٥٥٧
٥٥٨

٥٥٩ Table.2

Parameters	**(linear parallel bond model)**
Inter-particle elasticity modulus, E^*: MPa	400
Normal-to-shear stiffness ratio, κ^*	0.25
Inter-particle friction, μ	1
The inter-particle elasticity modulus of parallel bond, E_{pb}: Mpa	400
Normal-to-shear stiffness ratio of parallel bond, κ_{pb}	0.25
Friction angle of parallel bond, $\phi°_{pb}$	40°
The cohesion of the parallel bond, C_{pb}: Gpa	4×10^5
Tensile strength of the parallel bond, t_{pb}: Gpa	4000

٥٦٠ Table.3

Slab rotation	**Damage level**
$\mathbf{0° \leq \theta < 1°}$	**Slight**
$\mathbf{1° \leq \theta < 2°}$	**Moderate**
$\mathbf{2° \leq \theta < 5°}$	**Severe**
$\mathbf{\theta \geq 5°}$	**Threatening stability**

٥٦١ Table.4

Soil type	**Foundation Type**	**s/b**	**h/H (%) corresponding to the 2° rotations of the foundation**
Loose Soil (DR = 60%)	Light (q = 81 kPa)	-0.25	8.98
		0.00	12
		0.25	16.07
		0.50	>20
		0.75	>20
		1.00	>20
	Heavy (q = 162 kPa)	-0.25	11.55
		0.00	14.06
		0.25	19.91
		0.50	>20
		0.75	>20
		1.00	>20
Dense Soil (DR = 95%)	Light (q = 81 kPa)	-0.25	10.14
		0.00	12.93
		0.25	16.57
		0.50	>20
		0.75	>20
		1.00	>20
	Heavy (q = 162 kPa)	-0.25	12.95
		0.00	15.37
		0.25	19.02
		0.50	>20
		0.75	>20
		1.00	>20

٥٦٢
٥٦٣

٥٦٤
٥٦٥

٥٦٦ Table.5

Soil type	Foundation Type	s/b	h/H (%) corresponding to the 2° rotations of the foundation
Loose Soil (DR = 60%)	Light (q = 81 kPa)	-0.25	5.95
		0.00	10.5
		0.25	15.28
		0.50	>20
		0.75	>20
		1.00	>20
	Heavy (q = 162 kPa)	-0.25	10.76
		0.00	14.37
		0.25	19.28
		0.50	>20
		0.75	>20
		1.00	>20
Dense Soil (DR = 95%)	Light (q = 81 kPa)	-0.25	5.63
		0.00	13.56
		0.25	>20
		0.50	>20
		0.75	>20
		1.00	>20
	Heavy (q = 162 kPa)	-0.25	13.42
		0.00	8.53
		0.25	>20
		0.50	>20
		0.75	>20
		1.00	>20

٥٦٧ Table.6

Soil type	Foundation Type	s/b	h/H (%) corresponding to the 2° rotations of the foundation
Loose Soil (DR = 60%)	Light (q = 81 kPa)	-0.25	5.28
		0.00	6.98
		0.25	14.62
		0.50	>20
		0.75	>20
		1.00	>20
	Heavy (q = 162 kPa)	-0.25	7.78
		0.00	12.41
		0.25	19.15
		0.50	>20
		0.75	>20
		1.00	>20
Dense Soil (DR = 95%)	Light (q = 81 kPa)	-0.25	5.22
		0.00	9.1
		0.25	16.15
		0.50	>20
		0.75	>20
		1.00	>20
	Heavy (q = 162 kPa)	-0.25	9.39
		0.00	15.93
		0.25	>20
		0.50	>20
		0.75	>20

		1.00	>20

٥٦٨

Table.7

Soil type	Foundation Type	s/b	h/H (%) corresponding to the 2° rotations of the foundation
Loose Soil (DR = 60%)	Light (q = 81 kPa)	-0.25	5.54
		0.00	6.55
		0.25	8.96
		0.50	16.93
		0.75	>20
		1.00	>20
	Heavy (q = 162 kPa)	-0.25	10.56
		0.00	9.6
		0.25	13.3
		0.50	>20
		0.75	>20
		1.00	>20
Dense Soil (DR = 95%)	Light (q = 81 kPa)	-0.25	6.56
		0.00	5.22
		0.25	5.73
		0.50	19.5
		0.75	>20
		1.00	>20
	Heavy (q = 162 kPa)	-0.25	7.84
		0.00	7.5
		0.25	12.94
		0.50	>20
		0.75	>20
		1.00	>20

٥٦٩

Table.8

Soil type	Foundation Type	s/b	h/H (%) corresponding to the 2° rotations of the foundation
Loose Soil (DR = 60%)	Light (q = 81 kPa)	-0.25	5.49
		0.00	5.47
		0.25	8.03
		0.50	11.73
		0.75	>20
		1.00	>20
	Heavy (q = 162 kPa)	-0.25	5.69
		0.00	11.68
		0.25	12.18
		0.50	>20
		0.75	>20
		1.00	>20
Dense Soil (DR = 95%)	Light (q = 81 kPa)	-0.25	8.67
		0.00	6.32
		0.25	6.27
		0.50	10.33
		0.75	>20
		1.00	>20
	Heavy (q = 162 kPa)	-0.25	10.3
		0.00	12.98
		0.25	11.82
		0.50	14.88
		0.75	>20
		1.00	>20

Table.9

Soil type	Foundation Type	s/b	h/H (%) corresponding to the 2° rotations of the foundation
Loose Soil (DR = 60%)	Light (q = 81 kPa)	-0.25	4.1
		0.00	5.07
		0.25	8.3
		0.50	13.83
		0.75	>20
		1.00	>20
	Heavy (q = 162 kPa)	-0.25	5.92
		0.00	6.5
		0.25	12.9
		0.50	18.37
		0.75	>20
		1.00	>20
Dense Soil (DR = 95%)	Light (q = 81 kPa)	-0.25	7.17
		0.00	4.86
		0.25	4.15
		0.50	6.93
		0.75	>20
		1.00	>20
	Heavy (q = 162 kPa)	-0.25	8.06
		0.00	7.01
		0.25	8.52
		0.50	14.47
		0.75	>20
		1.00	>20

Figure caption list

Figure.1. Soil-shallow foundation-reverse fault model geometry, boundary conditions
Figure.2. PSDs of Firoozkoh sand No. 161 and the DEM simulation
Figure.3. Comparison of numerical and experimental results of the rupture surfaces of reverse fault with β=75° without the foundation: (a) the experimental study [36]; (b) the DEM simulation of particles with a rotation exceeding 0.5 radians; (c) Vertical displacements of ground surface for reverse faults of numerical and experimental model
Figure.4. Comparison of numerical and experimental results of the rupture surfaces of reverse fault with β=60° with the foundation: (a) the experimental study [24]; (b) the DEM simulation of particles with a rotation exceeding 0.5 radians; (c) Foundation rotation of numerical and experimental model
Figure.5. Variation of the Rave during the faulting: (a) Without foundation; (b) With foundation
Figure.6. Using Particles with a rotation exceeding 0.5 radians to Depict the Propagation of fault ruptures in models after the faulting process with β = 15°
Figure.7. Using Particles with a rotation exceeding 0.5 radians to Depict the Propagation of fault ruptures in models after the faulting process with β = 30°
Figure.8. Using Particles with a rotation exceeding 0.5 radians to Depict the Propagation of fault ruptures in models after the faulting process with β = 45°
Figure.9. Using Particles with a rotation exceeding 0.5 radians to Depict the Propagation of fault ruptures in models after the faulting process with β = 60°
Figure.10. Using Particles with a rotation exceeding 0.5 radians to Depict the Propagation of fault ruptures in models after the faulting process with β = 75°
Figure.11. Using Particles with a rotation exceeding 0.5 radians to Depict the Propagation of fault ruptures in models after the faulting process with β = 90°

Figures

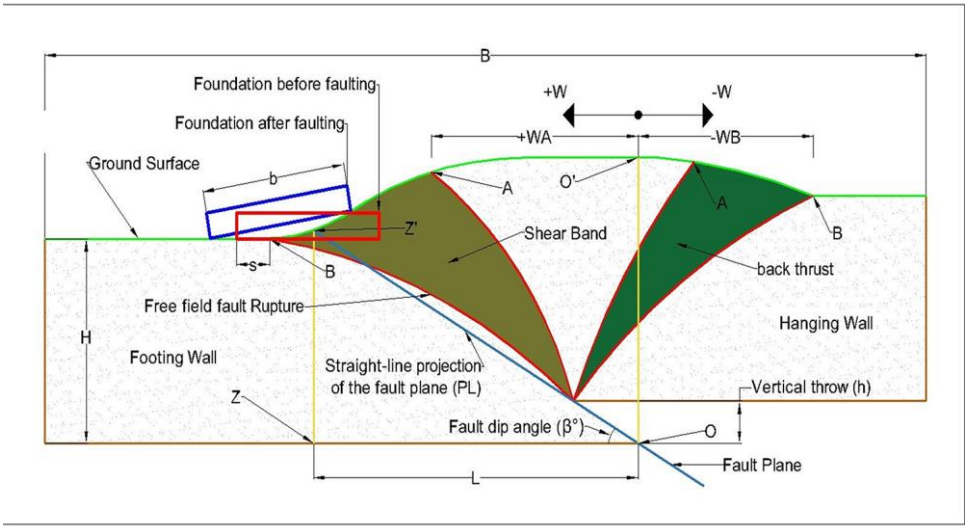

Figure.1

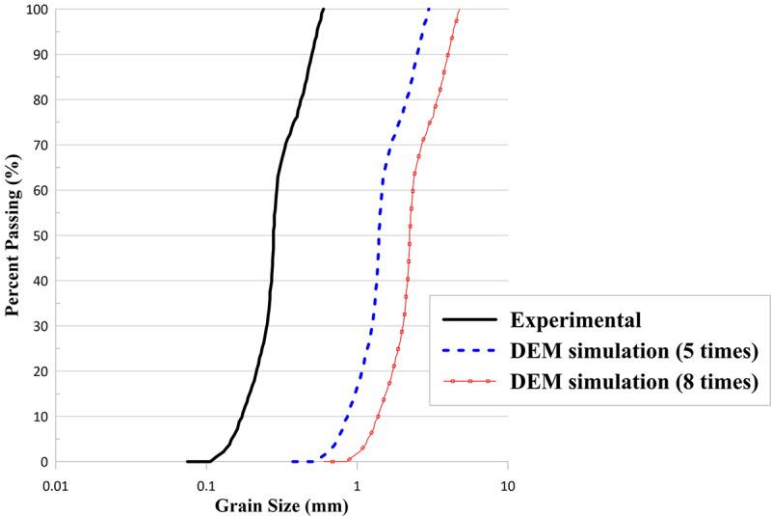

Figure.2

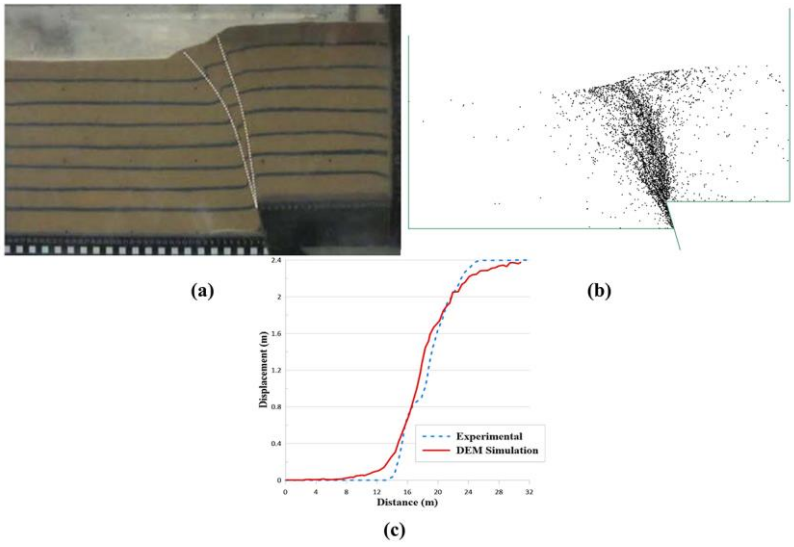

٦٠٠

٦٠١ Figure.3

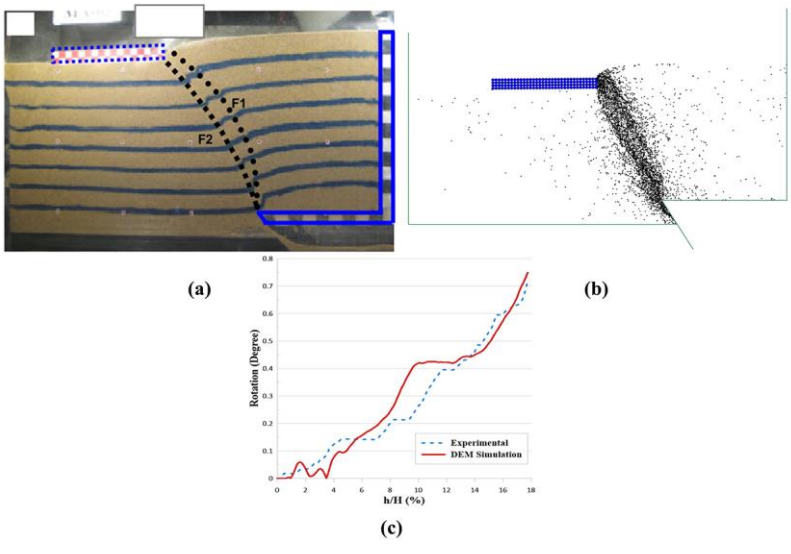

٦٠٢

٦٠٣ Figure.4

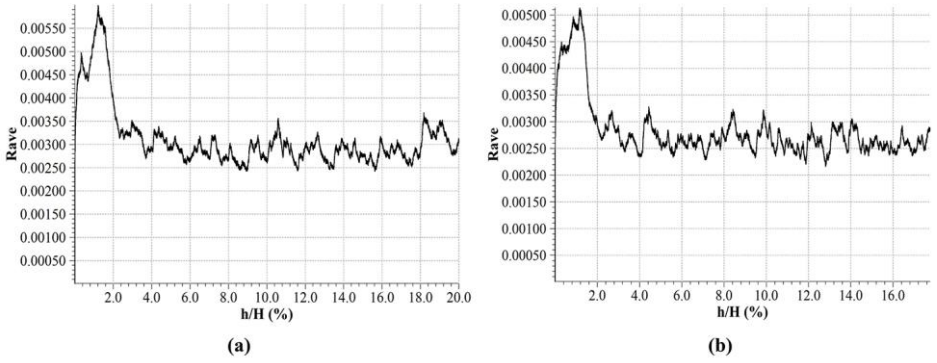

٦٠٤

٦٠٥ Figure.5

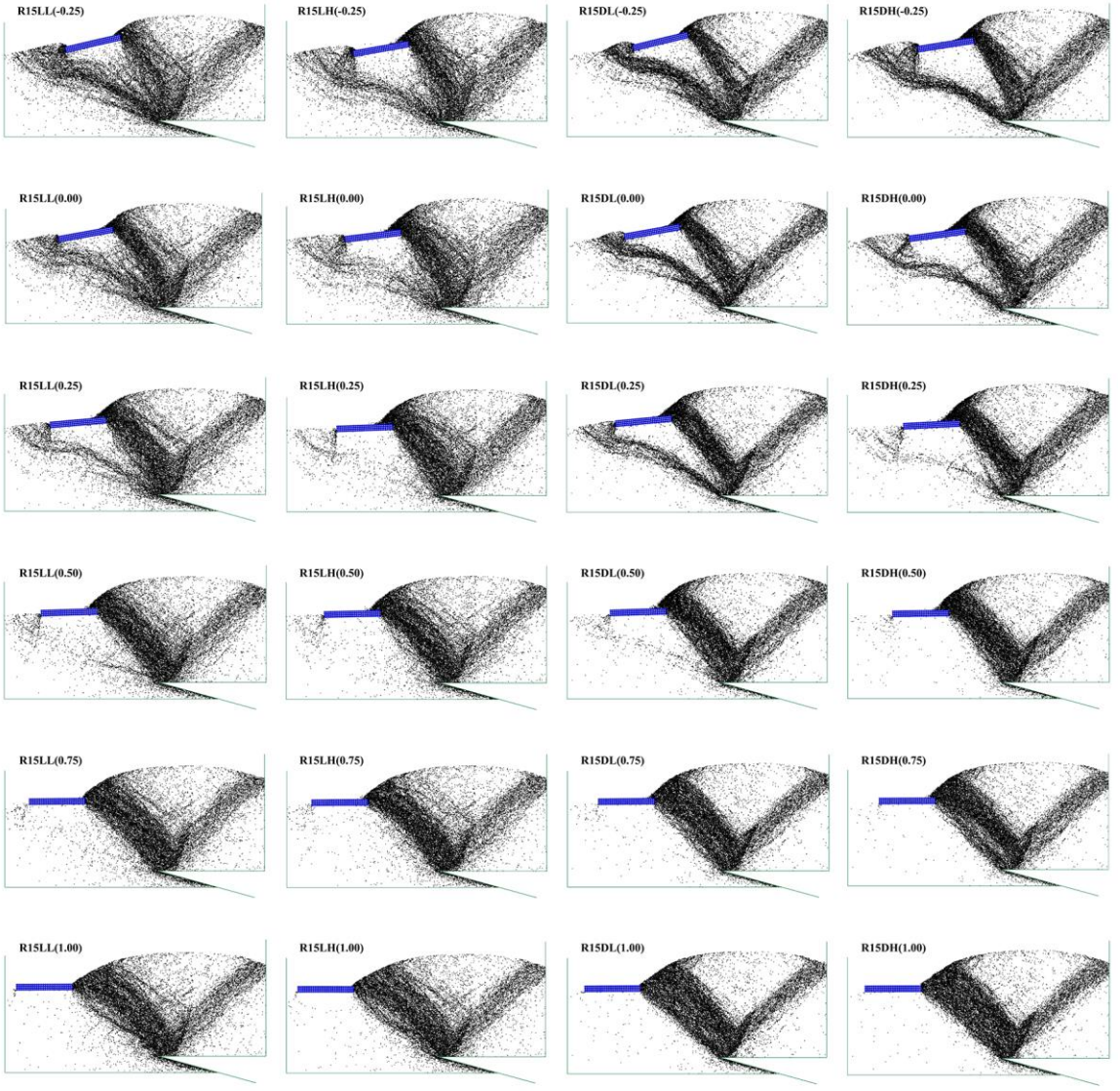

٦٠٦

٦٠٧ Figure.6

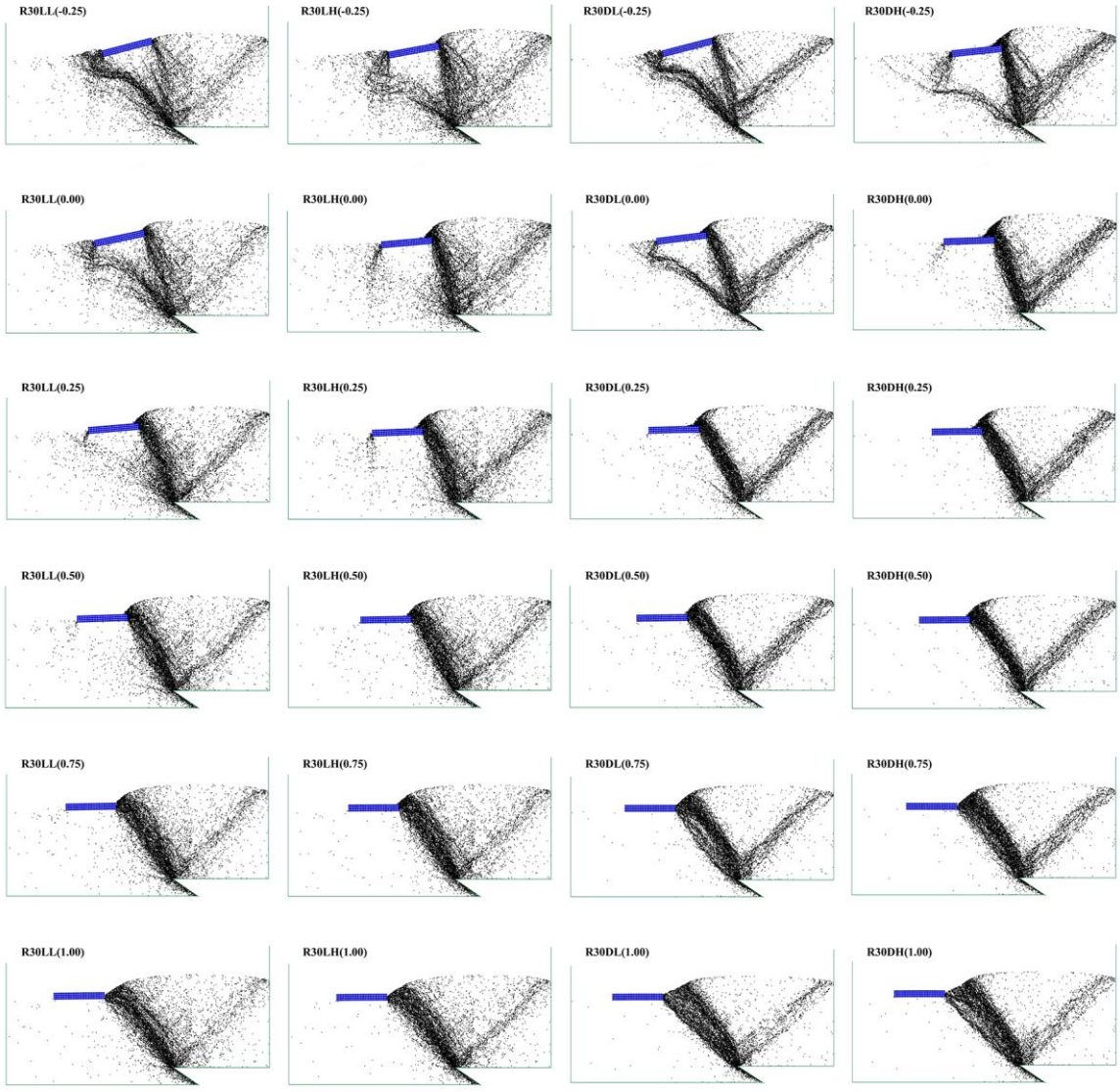

٦٠٨

٦٠٩

Figure.7

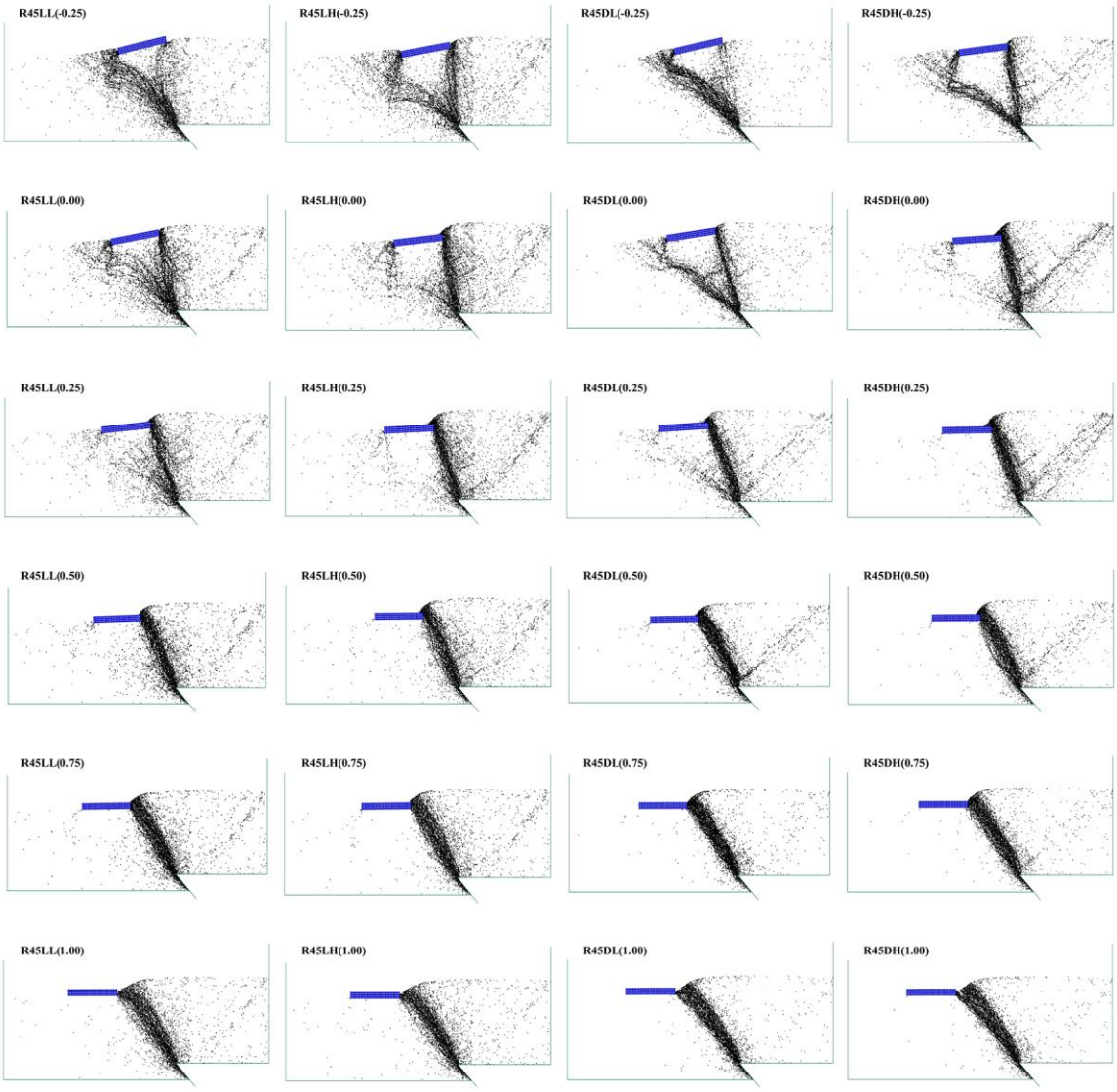

٦١٠

٦١١ Figure.8

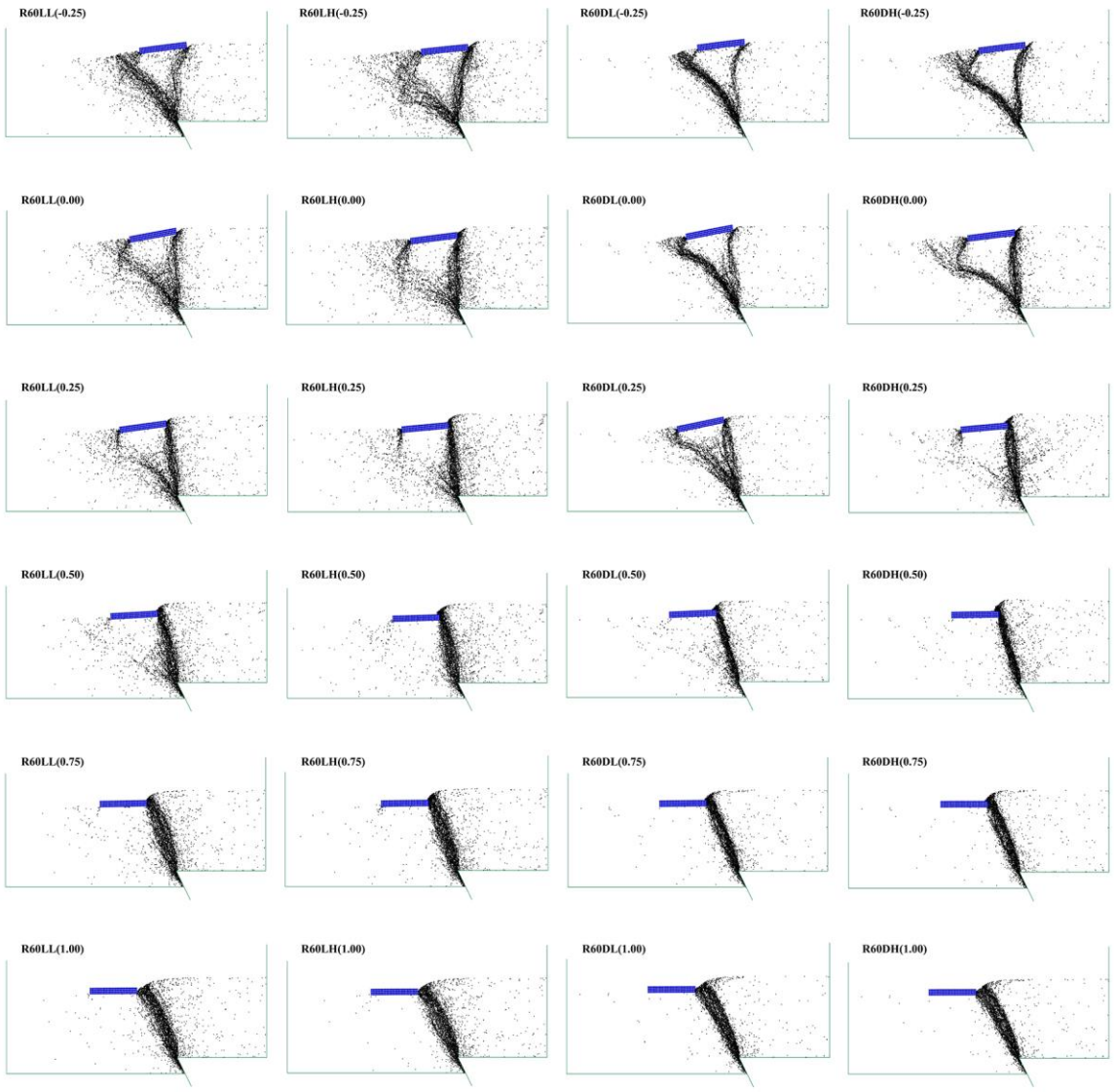

٦١٢

٦١٣ Figure.9

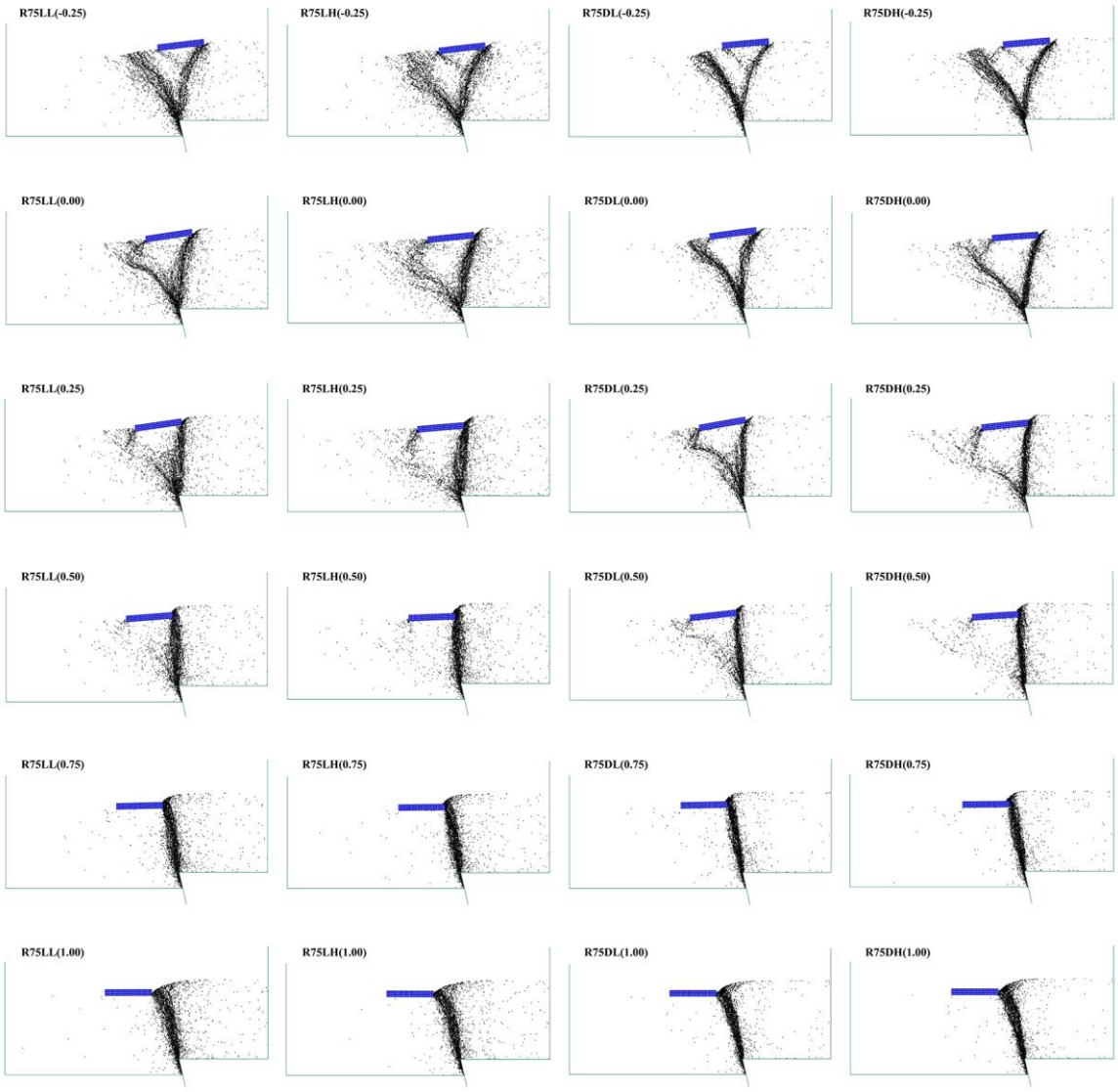

٦١٤

٦١٥ Figure.10

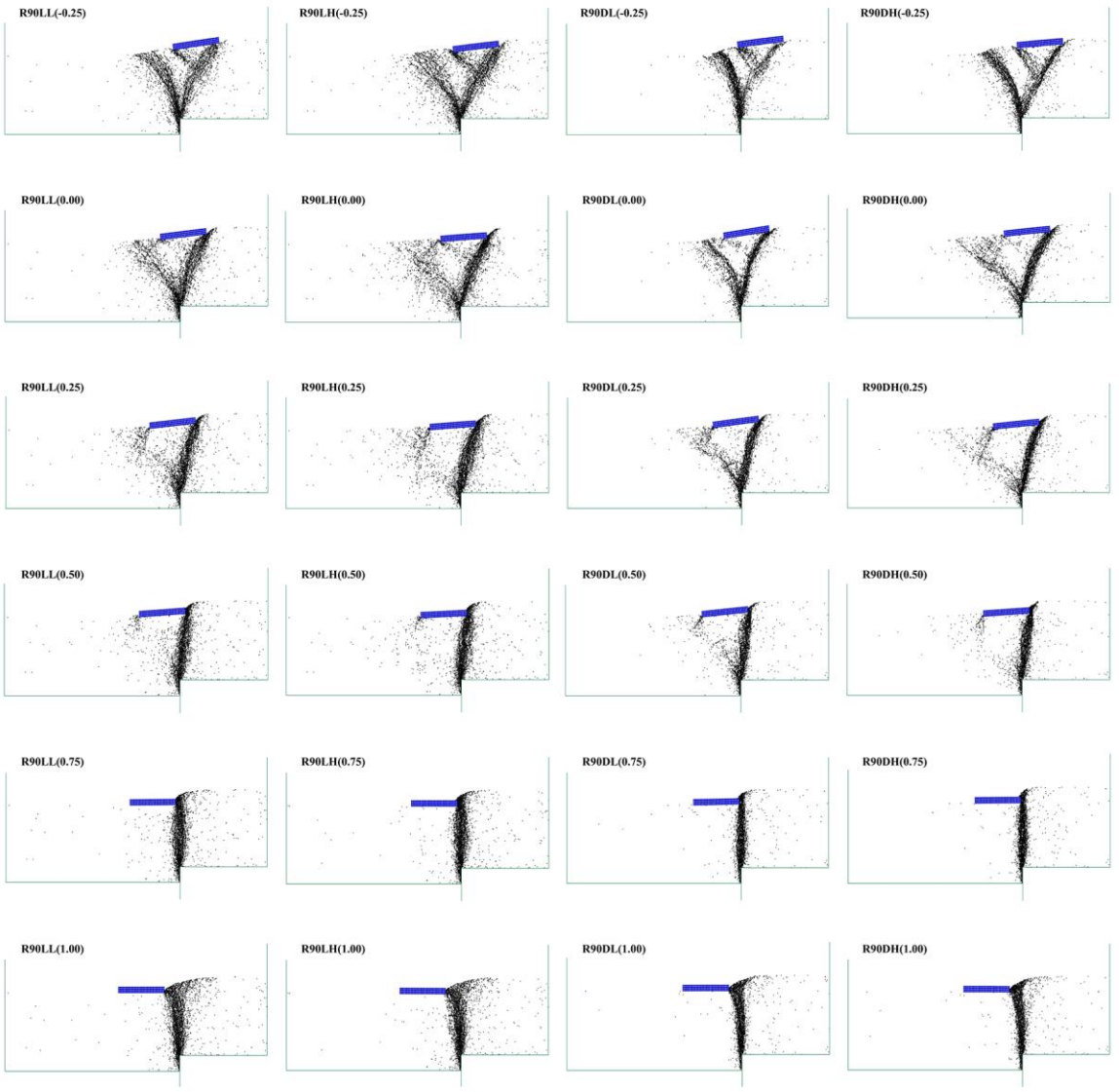

Figure.11

Author 1

- **Saman Ghaderi**

Mr. Ghaderi, a graduate of the University of Kurdistan, Sanandaj (B.Sc. Civil Engineering) and Iran University of Science and Technology (M.Sc. Geotechnical Engineering), is currently a Ph.D. student of Geotechnical Engineering at the Iran University of Science and Technology.

His research is focused on Discrete Element Modeling and Micromechanics of Dip-Slip Faulting - Shallow Foundation Interaction and Mitigation Procedures.

His current Ph.D. thesis and research focuses on Liquefaction Improvement With Soil Cement Columns, Cyclic Softening of Fine Grain Soil, and Phase Transformation During Liquefaction.

For more info visit: https://www.linkedin.com/in/saman-ghaderi-5783b8156/

Author 2

- **Amir Mohammad Fahmi**

Mr. Fahmi, a graduate of Kharazmi University (B.Sc. Civil Engineering) and Iran University of Science and Technology (M.Sc. Geotechnical Engineering), is currently a master's student of Subsurface Engineering at Ruhr University Bochum.

His research is focused on Discrete Element Modeling and Micromechanics of Pile Bearing Capacity Interaction with Voids in Different Soils.

For more info visit: https://www.linkedin.com/in/amirmohammadfahmi/

Author 3

- **Alireza Saeedi Azizkandi**

Dr. Alireza Saeedi Azizkandi is an Associate Professor in Geotechnical and Geoenvironmental Engineering at Iran University of Science and Technology. He holds a Ph.D. from Iran University of Science and Technology, focusing on physical modeling (shaking table and centrifuge), numerical analysis, and earth dam analysis.

His research includes Discrete/Finite Element Modeling, Parallel Programming, and Cluster Computing. Dr. Saeedi Azizkandi Teaches Soil Mechanics, Foundation Engineering, and Advanced Soil Mechanics.

For more info visit: https://civil.iust.ac.ir/content/49786/Dr.-Saeedi-Azizkandi,-Alireza